The pivotal role of copper(II) in the enantiorecognition of tryptophan and histidine by gold nanoparticles

ARTICLE *in* ANALYTICAL AND BIOANALYTICAL CHEMISTRY · NOVEMBER 2013

Impact Factor: 3.44 · DOI: 10.1007/s00216-013-7466-0 · Source: PubMed

6 AUTHORS, INCLUDING:

Annalinda Contino
University of Catania
54 PUBLICATIONS **1,248** CITATIONS
SEE PROFILE

Massimo Zimbone
Italian National Research Council
43 PUBLICATIONS **93** CITATIONS
SEE PROFILE

Alessandro Giuffrida
University of Catania
33 PUBLICATIONS **492** CITATIONS
SEE PROFILE

Anal Bioanal Chem (2014) 406:481–491
DOI 10.1007/s00216-013-7466-0

RESEARCH PAPER

The pivotal role of copper(II) in the enantiorecognition of tryptophan and histidine by gold nanoparticles

Annalinda Contino · Giuseppe Maccarrone · Massimo Zimbone · Paolo Musumeci · Alessandro Giuffrida · Lucia Calcagno

Received: 15 July 2013 / Revised: 23 October 2013 / Accepted: 25 October 2013 / Published online: 15 November 2013

Abstract Stereoselective amino acid analysis has increasingly moved into the scope of interest of the scientific community. In this work, we report a study on the chiral recognition of D,L-Trp and D,L-His using L-Cys-capped gold nanoparticles (AuNPs) and copper(II) ion. In the L-Cys-capped AuNPs, the thiol group of the amino acid interacts with AuNPs through the formation of Au–S bond, whereas the α-amino and α-carboxyl groups of the surface-confined cysteine can coordinate the copper(II) ion, which in turn, binds the L- or D-amino acid present in solution forming diastereoisomeric complexes. The resulting systems have been characterized by UV–Vis spectra and dynamic light scattering measurements, obtaining different results for L- and D-Trp, as well as for L- and D-His. The knowledge of the solution equilibria of the investigated systems allowed us to accurately calculate in advance the concentrations of the species present in solution and to optimize the system performances, highlighting the pivotal role of copper(II) ion in the enantiodiscrimination processes.

Keywords Chiral analysis · Gold nanoparticles · Solution equilibria · Copper(II) · Amino acids

A. Contino (✉) · G. Maccarrone
Dipartimento di Scienze Chimiche, Università degli Studi di Catania, Viale A. Doria 6, 95125 Catania, Italy
e-mail: acontino@unict.it

M. Zimbone · P. Musumeci · L. Calcagno
Dipartimento di Fisica e Astronomia, Università degli Studi di Catania, Via S. Sofia 64, 95123 Catania, Italy

A. Giuffrida
Istituto di Biostruttura e Bioimmagini, CNR, Viale Andrea Doria 6, 95125 Catania, Italy

Introduction

Chiral molecules in living organisms in nature exist almost exclusively as single enantiomers, a property that is critical for molecular recognition and replication processes and would thus seem to be a prerequisite for the origin of life [1]. The living world is chiral-selective, exhibiting different physiological responses to different enantiomers. Among bioactive molecules, amino acids (AAs) most exist in an L- and a D-form and, thanks to the recent advancement in stereoselective amino acid analysis [2, 3], the idea that in higher organisms only their L-enantiomers are of relevance gave way to the evidence that the D-forms of certain amino acids are widely present in tissues and body fluids of mammalians. In this respect, D-amino acids can function [4–6] as biomarkers for the diagnosis of pathological conditions, as for the Alzheimer disease in the pre-dementia phase or, ideally, in pre-symptomatic individuals [7, 8] since differences in the levels of L- and D-amino acids are clearly observed among the sample of cerebrospinal fluid pools from different patients [9]. Furthermore, the discrimination of amino acid enantiomers plays a relevant role in the fields of pharmaceutical science and biochemistry [10]. In particular, L-tryptophan in addition to be a component of proteins and neuropeptides [11] and the precursor for several biologically active compounds, as, for example, the kynunerine [12], is closely related to several chronic diseases and used as pharmaceutical antidepressant agent and as an efficacious treatment for chronic insomnia [13] whereas D-Trp has no significant biological effects. Similarly, the effect of histidine on the in vivo intestinal zinc absorption was stereospecific: L-histidine maintains quantitative zinc uptake, whereas the retained or absorbed Zn(II) fractions in the presence of D-histidine are significantly lower [14]. Moreover, L- and D-His were used to investigate chiral selection by D-ribose RNA [15]. Thus, the selective discrimination of the Trp and His enantiomers is of great importance.

Gold nanoparticles (AuNPs) have unique properties, such as size- and shape-dependent optical and electronic features, a high surface area to volume ratio, and surfaces that can be readily modified with ligands containing functional groups such as thiols, phosphines, and amines, which exhibit affinity for gold surfaces [16]. Owing to these unique properties, AuNPs have many applications in diagnostics and therapeutics [17], catalysis [18], optical sensing [19], and as biomarkers and building blocks in nanotechnology. On the other hand, among all forms of catalytic selectivity, enantioselectivity is perhaps the most subtle and the most difficult to control.

The functionalization of nanoparticles by chiral molecules has been recently exploited for enantiodiscrimination [20–22]. In fact, as elegantly demonstrated by the team of Govorov [23], chiral molecules are shown to induce circular dichroism (CD) at surface plasmon resonances of gold nanostructures when in proximity to the metal surface even without direct bonding to the metal. Thus, the chirality of the ligands is transferred to the metal core either in its structure or at least in its electronic states via perturbation of the electronic field of the ligands. Thus, CD has been widely exploited in this field [23], often providing detailed information on the investigated systems, even though its use requires expensive instrumentation and skilled and trained researchers and it does not provide results of outstanding interpretability.

On the other hand, functionalized gold nanoparticles have been increasingly explored as colorimetric sensors due to their remarkable photophysical and photochemical properties and thus can be good candidates for enantiorecognition of chiral biomolecules. The color changes are mainly due to aggregation phenomena that can be accurately described by using dynamic light scattering (DLS) investigations that allow to determine the hydrodynamic radii of the particles in solution. Furthermore, aggregation phenomena frequently give rise to changes of the SPR in the extinction spectra and thus can be elegantly modeled by considering solutions of the Maxwell equations such as those found in the Mie–Gans theory for spheres and ellipsoidal shaped nanoparticles [24] providing an accurate snapshot of the phenomena occurring in solution, as recently demonstrated by some of us [25].

In every technique utilized for enantiodiscrimination [26], the process responsible for the recognition and/or the separation of two enantiomers is the formation of diastereoisomeric complexes between the enantiomers and a chiral selector. In many cases, the presence of a metal ion favors these interactions by the formation of ternary complexes and makes extremely tunable the processes occurring in solution, allowing to maximize the difference in the degree of formation between the resulting diastereoisomeric complexes and thus to optimize the discrimination process [27–29].

Some of us have an acknowledged expertise in the field of enantiomeric discrimination of derivatized [30] and underivatized [31] amino acids by using capillary electrophoresis techniques. In this context, the accurate characterization, carried out in advance, of the solution equilibria involved in the separation processes is crucial for the optimization of the experimental conditions [26], allowing a fine tuning of the processes themselves [32]. In fact, the exact knowledge of the composition of a solution can be used to predict the conditions required for the optimal formation of a given complex, giving great importance in planning separation procedures and dramatically improving their performances.

Exploiting these different and complementary expertise we now report a study on the enantiodiscrimination processes of underivatized D,L-Trp and D,L-His obtained by using AuNPs functionalized with L-Cys and the related amino acids copper(II) complexes. The properties of these systems have been investigated by using UV–Vis spectroscopy to determine the kinetics of the processes and the shape and the dimensions of the particles, as well as by DLS to evaluate their hydrodynamic radii. The main innovation of the paper consists in the use of copper(II) ion, as well as of the concerning solution equilibria data to fine tune and optimize the experimental conditions. Furthermore, we conjugate our experience in the investigation on the copper(II) complexes thermodynamic stereoselectivity with the expertise in UV–Vis spectroscopy and dynamic light scattering to obtain a careful inspection of the chiral recognition process. This approach would be easily extendible to develop simple, rapid and sensitive assays for chiral recognition.

Experimental part

Materials L-cysteine, L-alanine, D-alanine, L-tryptophan, D-tryptophan, L-histidine and D-histidine were obtained as commercial reagents by Merck and were used as received. $HAuCl_4 \cdot 3H_2O$ and trisodium citrate ($Na_3Cit \cdot 2H_2O$) were purchased from Sigma Aldrich. Copper(II) sulfate (Carlo Erba) stock solutions were standardized by EDTA titrations [33].

Synthesis of AuNPS The citrate-capped AuNPs were prepared by the citrate reduction method pioneered by Turkevich et al. [34], refined by Frens [35] and once for all described in details by Hill and Mirkin [36]. Shortly, to a 50-mL aqueous solution of 1.00 mM $HAuCl_4$ (whose concentration was determined by using the molar absorptivity reported by Wang et al. [37]) refluxed under stirring, 5.00 mL of an aqueous 38.8 mM sodium citrate solution was added. After 15.0 min, a wine red solution was obtained, that was allowed to cool to room temperature prior to being filtered using a 0.45 μm filter. Finally, as suggested by Sethi et al. [38], the solution was centrifuged at 5,000 rpm for 2.00 min, and the supernatant was studied. Two independent batches were synthesized, characterized, and utilized for the chiral recognition measurements.

Spectroscopic measurements

UV-spectra of the investigated systems were carried out at room temperature, using a diode-array Agilent 8453 spectrophotometer in the 400–900 nm wavelength. The concentration of the AuNPs solutions was calculated by using the Beer's law ($\varepsilon = 2.01 \times 10^8$ cm^{-1} M^{-1}) according to Maye et al. [39]. The particle diameter (in nanometers) was calculated analyzing the UV-spectra by the Haiss method [40] by using the following relation:

$$d = \exp\left(B_1 \frac{A_{522}}{A_{450}} - B_2\right) \quad (1)$$

where $B_1 = 3.00$ and $B_2 = 2.20$ and A_{522} and A_{450} are the absorbance at 522 nm (SPR peak) and 450 nm, respectively.

UV–Vis chiral recognition The solution containing the AuNPs and L-Cys was prepared by diluting the appropriate amount of the gold colloid and of a 1 mM L-Cys stock solution, obtaining a concentration of 1.12 nM and 2.63×10^{-5} M for Au and cysteine, respectively. A volume of 1.1 ml of this solution was added to 1.4 ml of Cu(II) L-Ala, Cu(II) D-Ala, Cu(II) L-Trp, Cu(II) D-Trp, Cu(II) L-His or Cu(II) D-His complexes, to obtain a final concentration of 5.0×10^{-5} M and 1.0×10^{-4} M in copper(II) and in amino acid, respectively. Immediately the absorption reading was begun following a 90-min period and 3-min interval. Subsequently, a further addition of a copper sulfate solution was made to obtain a final 1.0×10^{-4} M copper concentration and another absorption reading was carried out following the same period and interval. Alternatively, the solution containing the AuNPs and L-Cys was prepared by diluting the appropriate amount of the gold colloid and of a 1 mM L-Cys stock solution, realizing a concentration of 0.88 nM and 2.63×10^{-5} M for Au and cysteine, respectively. 1.0 ml of this solution was added to 1.5 ml of Cu(II) L-Ala, Cu(II) D-Ala, Cu(II) L-Trp, Cu(II) D-Trp, Cu(II) L-His or Cu(II) D-His complexes, to obtain a final concentration of 1.0×10^{-4} M in copper(II) and in amino acid, respectively.

The species distribution diagrams calculated for optimize the experimental conditions have been obtained by the simulation and speciation program HYSS [41].

DLS measurements

The DLS measurements were carried out by a homemade apparatus as described elsewhere [25]. The measurements were carried out 3 h after the preparation of the solution to allow the systems to react. The analysis of the fluctuations of the scattered light was performed by the intensity autocorrelation function (g_2). This autocorrelation function was provided by the hardware correlator operating in single photon counting regime. For monodisperse non-interacting particles in Brownian motion, the g_2 function is a decreasing exponential with a relaxation rate Γ ($\Gamma = 1/\tau$ with τ = decay time). Once the relaxation rate is obtained, it is possible to calculate either the translational diffusion coefficient (D_t) and the hydrodynamic radius (R_H) using the following expressions [42]:

$$\Gamma = D_t q^2 \quad (2)$$

where q is the scattering vector, defined as $q = (4\pi n/\lambda)\sin(\theta/2)$, being n the refraction index of the solvent, λ the light wavelength, θ the scattering angle,

and,

$$R_H = kT/(6\pi\eta D_t) \quad (3)$$

where η is the liquid viscosity, k the Boltzmann constant, and T the absolute temperature. We used a scattering angle $\theta = 90°$.

Results and discussion

The UV–Vis spectrum of the citrate-capped Au nanoparticles (NPs) is reported in Fig. 1a. The spectrum exhibit only a single peak ($\lambda_{spr} = 522$ nm), indicating that the solution contains highly dispersed Au nanoparticles. In order to carry out the measurements with a high degree of reproducibility, we estimated the concentration values (calculated by the absorbance values) of the solutions obtained after the filtration, as well as the diameter values of the nanoparticles by using the Haiss method. The two batch give rise to a concentration of 17.6 nM and a diameter value of 16±1 nm, for the batch I and a concentration of 16.5 nM and a diameter value of 19±1 nm, for the batch II, respectively.

In Fig. 1a is also reported the UV–Vis spectrum of the L-cysteine-capped AuNPs recorded immediately after the preparation and after a period of aging of ca. 1 month. Thiol-containing amino acid show high affinity towards the surface of gold nanoparticles [43] as can be finely described by the hard–soft acid–base theory [44], that find applicability also in such a microenvironment [45]. Thus, owing to its high affinity, L-Cys is reported to induce gold [46–48] and silver [49] nanoparticles aggregation, mainly at acidic pH values. In spite of this, by using a low L-Cys concentration ($1.0–3.0 \times 10^{-5}$ M) and a fine control of the pH, we prevented particles aggregation and obtained again a highly dispersed AuNPs solution, as evidenced by the fact that the spectra of the citrate-capped and cysteine-capped AuNPs do not show significant differences with the exception of a slight shift of the surface plasmon band from 522 to 520 probably due to the damping effect of the thiol group on the gold surface [50, 51]. Furthermore, the

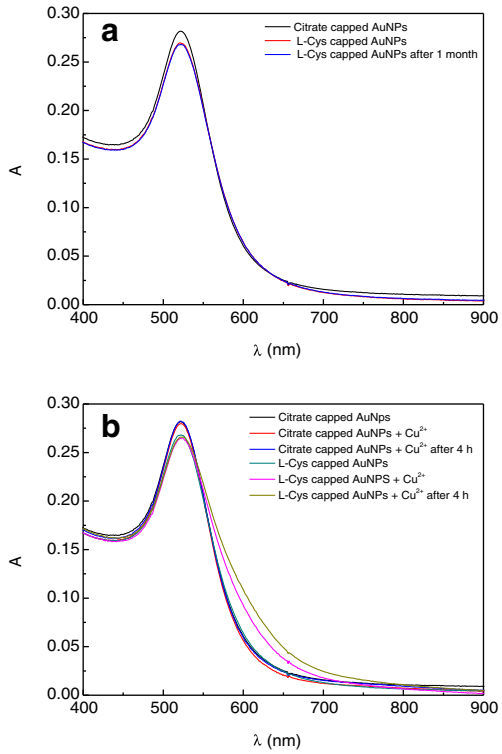

Fig. 1 UV–Vis spectra recorded for **a** citrate-capped and L-Cys-capped AuNPs; **b** citrate-capped and L-Cys-capped AuNPs in the absence and in the presence of copper(II)

spectrum recorded after a month is superimposable with that obtained immediately after the preparation (Fig. 1a), showing that the L-Cys Au colloid is stable for several weeks.

In Fig. 1b are reported the UV–Vis spectra of the citrate-capped AuNPs, as well as of the L-Cys-capped ones in the absence and in the presence of copper(II) at the concentration utilized for the enantiodiscriminination experiments. Also, Cu^{2+} ion is reported to promote the aggregation of citrate-capped AuNPs at a concentration of 2.0×10^{-4} M and at pH> 5.5–6.0 [52], as well as of the L-Cys-capped ones at a concentration of 6.0×10^{-4} M [45]. However, as evidenced in Fig. 1b, we did not find aggregation processes exclusively imputable to the Cu^{2+} ion at the concentrations utilized in our experiments, that anyway are lower than those reported in references 51 and 52, as well as the measured pH of the final solutions never exceeds the value of 6.0. In the presence of both copper(II) and L-Cys we only find a little change in the shape of the plasmon peak imputable to a slight aggregation process. Anyway, 4 h after the preparation of the solution, the spectrum is only slightly different from that recorded before and thus this aggregation cannot interfere with the enantiodiscrimination process.

In the L-Cys-capped AuNPs, the thiol group of the amino acid interacts with AuNPs through the formation of Au–S bond, whereas the α-amino and α-carboxyl groups of the surface-confined cysteine can coordinate the copper(II) ion present in solution by forming a five-membered ring (Scheme 1). However, the coordination sphere of the metal ion is not complete and thus Cu^{2+} can be either complexed by another L-Cys-capped AuNP, giving rise to the well-known aggregation processes reported in the literature or by a different L- or D-amino acid present in solution (see Scheme 1). Obviously, the resulting diastereoisomeric complexes, due to the presence of two chiral centers in the adducts, should have different chemical–physical properties, giving rise to different behaviors. In order to favor routes II and III of Scheme 1, i.e., the formation of complexes with the amino acids to enantiodiscriminate, we added the L-Cys-capped AuNPs to a solution containing the copper(II) and L- or D-Ala or L- or D-Trp or L- or D-His in a ratio 1:1 or 1:2. In this way, as indicated in Fig. 2 that reports the species distribution diagram calculated for the system Cu(II)/L-Trp as an example at the concentrations used in our experiments, at the investigated pH (pH=6.0) more than 70 % of the total copper(II) in solution is present as L-Trp complexed species, thus favoring the enantiodiscrimination processes at the expense of the aggregation processes among the L-Cys-capped AuNPs, that are favored by the free copper in solution.

The diastereoisomeric complexes formed among the L-Cys-capped AuNPs, the Cu^{2+} ion and the L- or D-amino acids to enantiodiscriminate should also have different chemical–physical properties, giving rise to different behaviors. Our results confirm this trend: Fig. 3 shows the time course of the UV–Vis spectra for solutions containing Cu^{2+} ion and (a) L-Ala, (b) D-Ala, (c) L-Trp; (d) D-Trp, either in a 1:2 and a 1:1 ratio, whereas in the insets the concerning photographic images taken at the end of the reactions are shown. As widely described in the literature [53–58], alanine is not enantiodiscriminated by the formation of diastereisomeric complexes. In fact, owing to its short side chain, for the copper(II) alaninate ternary complexes, interligand interactions cannot occur and thus, as a consequence, stereoselectivity is either absent or insignificant. Analogously, the UV–Vis spectra of the Cys-capped AuNPs in presence of either L- or D-Ala are almost superimposable and the color of both solutions become blue (Fig. 3a and b), indicating that for both enantiomers an aggregation process is occurring.

On the contrary, the gold nanoparticles show high enantiodiscrimination capabilities towards L- or D-Trp (Fig. 3c and d). In fact, whereas for the system with L-Trp only a slight modification of the UV–Vis spectra is observed, the system with D-Trp is strikingly different. The plasmon absorption at 522 nm slightly decreases and a new absorption red shifted at 656 nm appears, indicating the occurrence of an aggregation process. Furthermore, AuNPs solutions also exhibit color changes: whereas the solution with L-Trp does not change its color, remaining red, the one with D-Trp exhibits a sensitive color change from red to blue, which can directly be seen with the naked eye (insets in Fig. 3c and d).

The processes described above are strongly dependent upon the copper(II) ion concentration. In fact, as shown in

Scheme 1 Different routes resulting in diastereoisomeric complexes

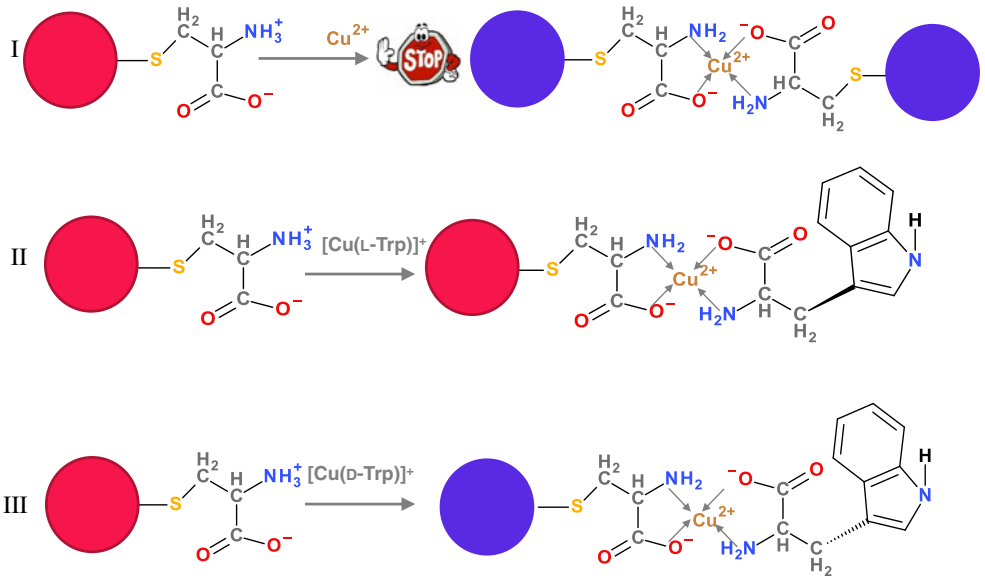

Fig. 4, that reports the spectra for the investigated systems at the end of the reactions, as well as the corresponding absorption ratios (A_{656}/A_{521}) as a function of time, almost no variation is observed at Cu(II)/amino acid ratio 1:2. Only when the metal ion concentration is raised to equal that of the amino acid to enantiodiscriminate, the aggregation processes start.

The L-Cys-capped AuNPs also show high enantiodiscrimination capabilities towards L- or D-His, those results are reported in Fig. 5, even though showing a different dependence on copper(II) ion concentration. In fact, for histidine, the enantiodiscrimination process become effective already at Cu/His ratio 1:2: the system with L-His shows only a slight modification of the UV–Vis spectra (Fig. 5a, light colors), whereas the system with D-His is strikingly different at this copper/amino acid ratio (Fig. 5b, light colors). On the other hand, the two systems show a nearly identical aggregation process when the metal ion concentration is raised to equal that of the amino acid to enantiodiscriminate (Fig. 3a and b, bright colors). The spectra for the investigated systems at the end of the reactions (Fig. 5c), as well as the corresponding absorption ratios (A_{656}/A_{521}) as a function of time (Fig. 5d), better underline the different dependence upon copper(II) concentration. Oppositely to L- and D-Trp systems that show no variation at a Cu(II)/amino acid ratio 1:2 (Fig. 4b), L- and D-His systems show the major variation at the lowest metal to ligand ratio, whereas the two diastereoisomeric complexes behave the same when the metal ion concentration is raised to equal that of the amino acid to enantiodiscriminate (Fig. 3c and d).

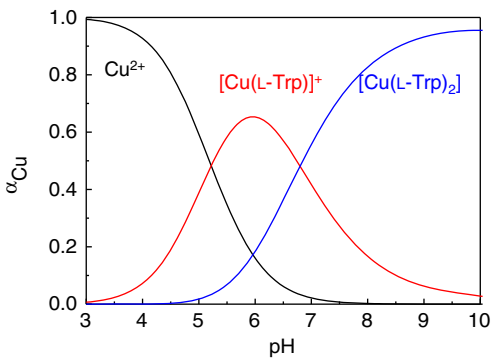

Fig. 2 Species distribution diagram for the system Cu(II)/L-Trp. Ccu=0.05 mM; CTrp=0.1 mM

Once again, the knowledge of the solution equilibria allows us to explain this behavior. In fact, besides copper(II), L-Cys and the amino acids to enantiodiscriminate, the final solutions contain citrate ions acting as capping agent for the AuNPs in a concentration range $3.00–3.30\times10^{-4}$ M. Considering that the concentration of AuNPs is about 0.35–0.45 nM and that each particle is surrounded by almost 3,000–4,000 citrate ions, as can be calculated considering a citrate footprint of 0.3 nm^2 [59], the citrate concentration is almost unaffected by the presence of the nanoparticles in solution and in large excess over the other ligands. In these experimental conditions, the copper(II) ion forms ternary complexes with L- or D-His and citrate [60]. In Fig. 6 are reported the species distribution diagrams for the ternary systems Cu/L-His/Cit calculated at the concentration used in our experiments. The diagrams show that, under the experimental conditions utilized in this work (pH=6.0), the complex with the highest degree of formation is the mixed species $[Cu(L\text{-}His)(Cit)]^{2-}$, that is the one that interacts with the cysteine bound on the AuNPs surface. Analogously, we could suppose that also in the systems Cu/L-Trp/Cit and Cu/D-Trp/Cit an analogous ternary species $[Cu(L\text{-}Trp)(Cit)]^{2-}$ or $[Cu(D\text{-}Trp)(Cit)]^{2-}$ is present and that also in this case this is the species that interacts with the cysteine bound on the AuNPs surface. As specified above, in the L-Cys-capped AuNPs, the thiol group of the amino acid interacts with AuNPs through the formation of Au–S bond,

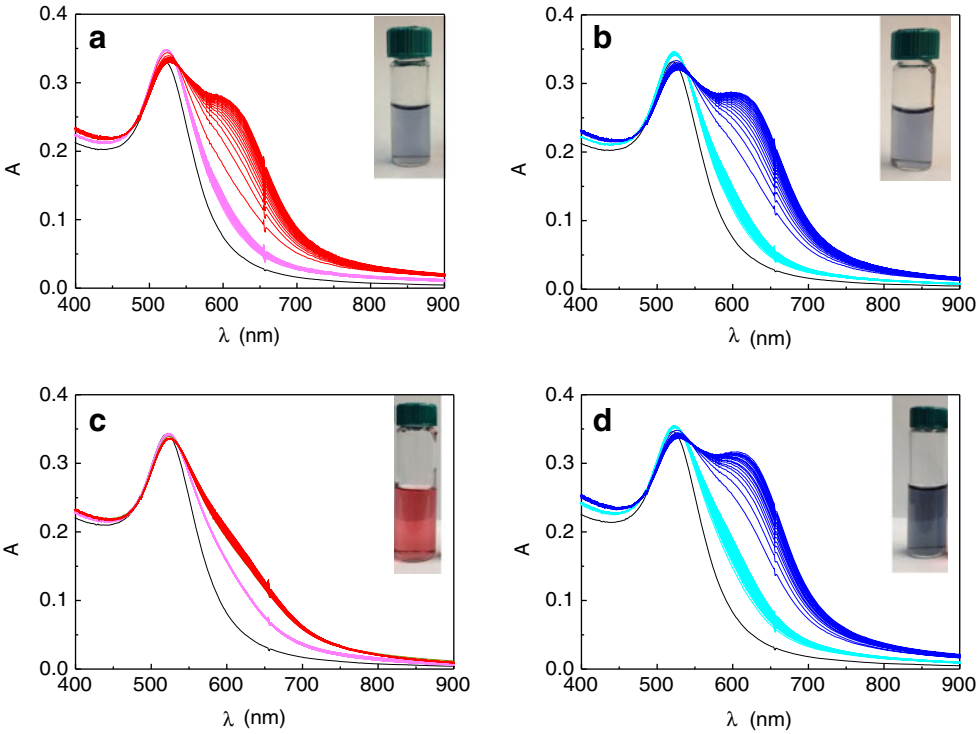

Fig. 3 Time course of the UV–Vis spectra for solutions containing AuNPs–L-Cys and **a** Cu^{2+} ion and L-Ala; **b** Cu^{2+} ion and D-Ala; **c** Cu^{2+} ion and L-Trp; **d** Cu^{2+} ion and D-Trp in a 1:2 (*light colors*) and a 1:1 ratio (*bright colors*). The spectrum of Cys-capped AuNPs is in *black* in all cases

whereas the α-amino and α-carboxyl groups of the surface-confined cysteine can coordinate the copper(II) ion present in solution, virtually behaving as alanine. This last amino acid has a major affinity towards copper(II) ion than citrate and thus could displace this last ligand giving rise to the diastereoisomeric complexes responsible for the enantiodiscrimination process observed. As shown in Fig. 6, raising the concentration of copper(II) ion from 5.0×10^{-5} M to 1.0×10^{-4} M, the degree of formation of the ternary species jumps from 30 to 50 %, promoting a better interaction of the amino acids to enantiodiscriminate with the L-Cys-capped AuNPs. Probably for the His systems this degree of formation results to be too high, leveling off any differences between the enantiomers to enantiodiscriminate. Thus, in this case, a lower

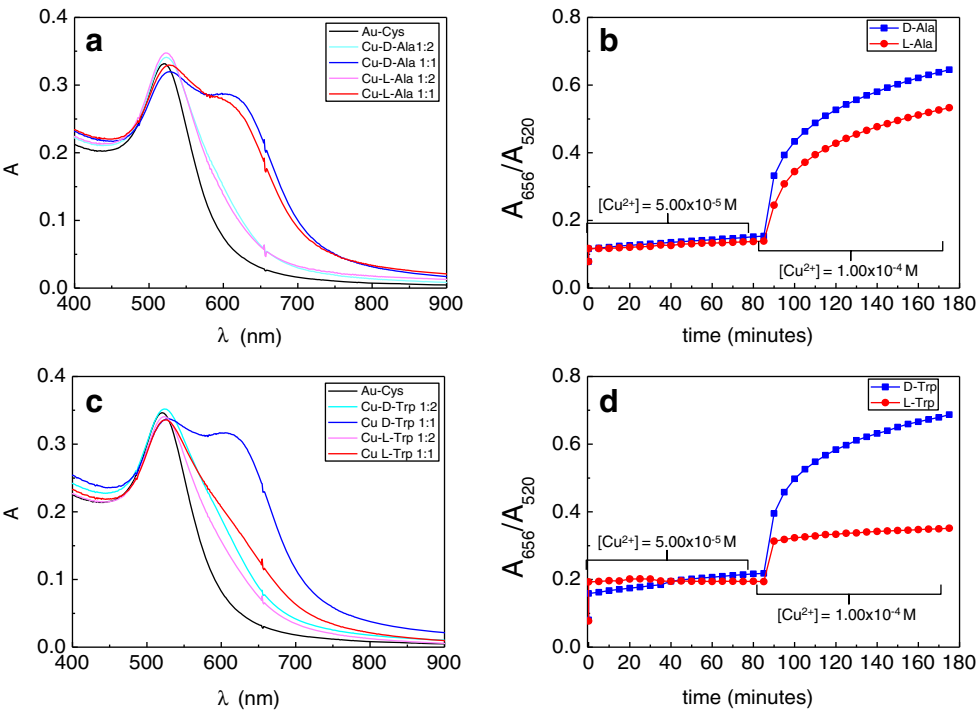

Fig. 4 UV–Vis spectra at the end of reaction and the corresponding plots of the absorption ratios (A_{656}/A_{521}) as a function of time for solutions containing AuNPs–L-Cys and **a** Cu^{2+} ion and L-Ala or D-Ala; **b** Cu^{2+} ion and L-Trp or D-Trp

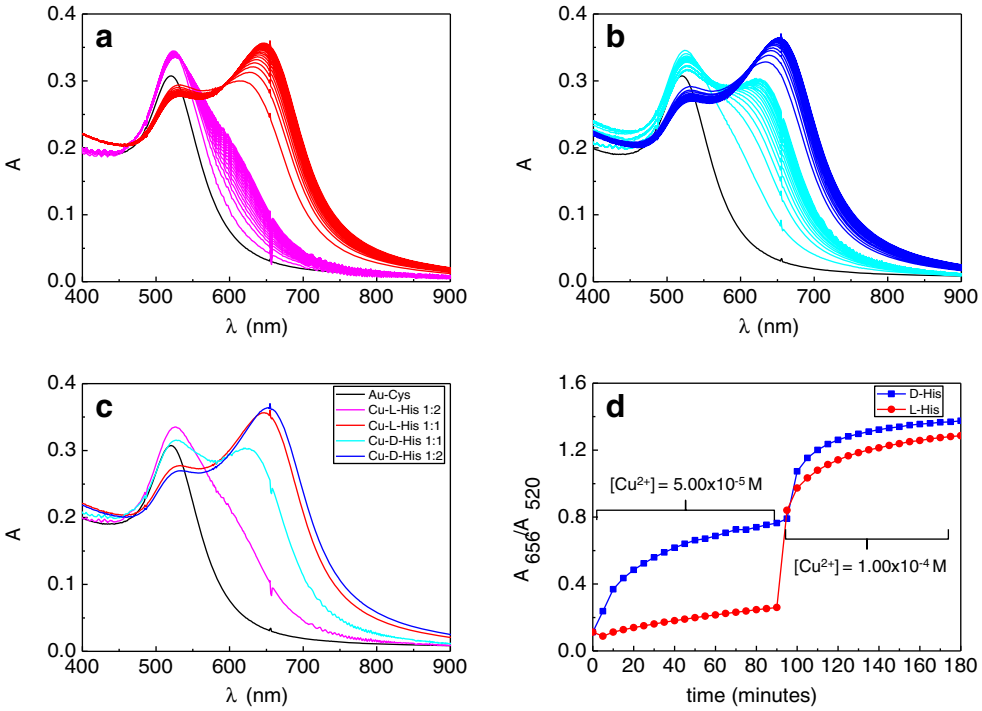

Fig. 5 Time course of the UV–Vis spectra for solutions containing AuNPs–L-Cys and **a** Cu^{2+} ion and L-His; **b** Cu^{2+} ion and D-His in a 1:2 (*light colors*) and a 1:1 ratio (*bright colors*). The spectrum of Cys-capped AuNPs is in *black* in all cases. **c** UV–Vis spectra at the end of reaction and **d** the corresponding plot of the absorption ratios (A_{656}/A_{520}) as a function of time for solutions containing AuNPs–L-Cys, Cu^{2+} ion and L-His or D-His

concentration of copper(II) ion and, as a consequence, of the ternary species $[Cu(L\text{-His})(Cit)]^{2-}$ and $[Cu(D\text{-His})(Cit)]^{2-}$ give rise to a better enantiodiscrimination. On the other hand, the L- and D-Trp systems do not show any significant difference at a Cu/Trp ratio 1:2. However, whereas for L- and D-Ala (Fig. 4a), even after a further addition of $CuSO_4$, the final spectra for the two enantiomers are practically superimposable, the final UV–Vis spectra for L- and D-Trp (Fig. 4b), after the copper(II) addition are remarkably different and the corresponding absorption ratio (A_{656}/A_{521}) show a sharp variation and a large difference between the two enantiomers. The opposite behavior of tryptophan and histidine is undoubtedly related to the different coordination characteristics of the two amino acids. In fact, whereas Trp is a bidentate ligand, His, in addition to the α-amino and α-carboxyl groups, has a further site of coordination, i.e., the imidazolic nitrogen atom and thus the $[CuHis]^{+}$ species shows an higher stability constant (log $K=10.15$) [60] than the corresponding $[CuTrp]^{+}$ species (log $K=8.29$) [61]. This stability difference (nearly 2 logarithmic units) probably affects the stability of the concerning ternary species and thus, to keep the degree of formation of the ternary species $[Cu(L\text{-Trp})(Cit)]^{2-}$ or $[Cu(D\text{-Trp})(Cit)]^{2-}$ sufficiently high to allow the enantiodiscrimination, we need an higher concentration of copper(II) ion.

In order to confirm the results obtained by UV–Vis spectra we carried out DLS measurements on the Ala and Trp systems. This technique, in fact, has been recently reported [62, 63] as suitable to determine the size as well as the shape of gold nanoparticles and nanoaggregates. The autocorrelation functions (g_2) of citrate-capped AuNPs, L-Cys-capped ones, as well as of Cu-L-Trp/L-Cys AuNPs and Cu-D-Trp/L-Cys AuNPs solutions are reported in Fig. 7a. The value of the

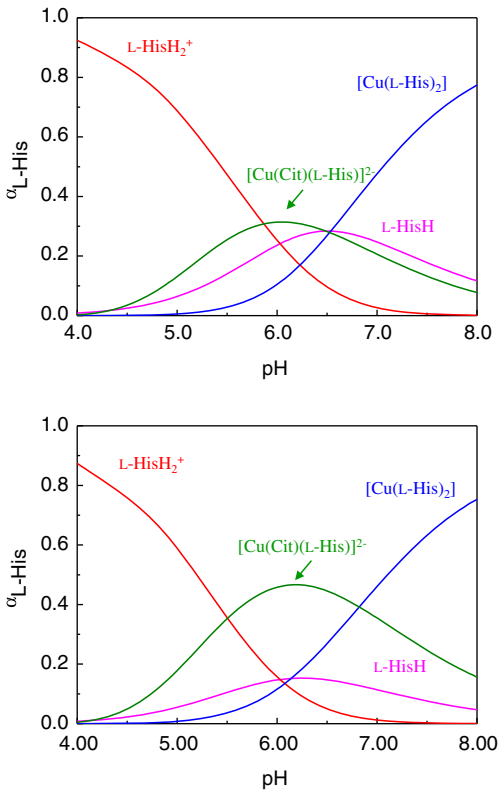

Fig. 6 Species distribution diagrams for the system Cu/Cit/L-His **a** $C_{Cu}=5\times10^{-5}$ M; $C_{Cit}=3\times10^{-4}$ M; $C_{L\text{-His}}=1\times10^{-4}$ M; **b** $C_{Cu}=1\times10^{-4}$ M; $C_{Cit}=3\times10^{-4}$ M; $C_{L\text{-His}}=1\times10^{-4}$ M

hydrodynamic nanoparticle radius calculated by cumulant analysis was 20 nm for the citrate-capped AuNPs and 21 nm for the L-Cys-capped ones. These values are slightly larger than the values obtained by UV–Vis spectroscopy. This discrepancy can be related both to the substances adsorbed on the nanoparticle surface (e.g., stabilizers) and to the thickness of the electrical double layer (solvation). Interestingly, whereas the hydrodynamic nanoparticle radius measured for the L-Cys–Au–L-Trp system is only slightly different from that of L-Cys-capped AuNPs (25 vs 21 nm), the corresponding value for the L-Cys–Au–D-Trp system is significantly different (38 nm), clearly indicating that in this case an aggregation process occurred.

In order to quantify the changes in the UV–Vis spectra due to aggregation phenomena, the Mie–Ganz model has been widely applied [64, 65]. This model considers the aggregates as object of elongated shape (ellipsoids) and shows that a spherical shaped metallic cluster, has a unique SPR peaked at about 520 nm while a prolate ellipsoid gives two characteristic extinction signals, one at the same frequency of the spherical particles, and the other red shifted. These two resonance frequencies are frequently referred to the plasmon resonance that occurs along the shorter axis and the longer axis of the ellipsoid.

The UV–Vis spectrum for the system AuNPs–L-Cys–Cu–L-Trp (Fig. 3c) shows an SPR at 522 nm, whereas the spectra

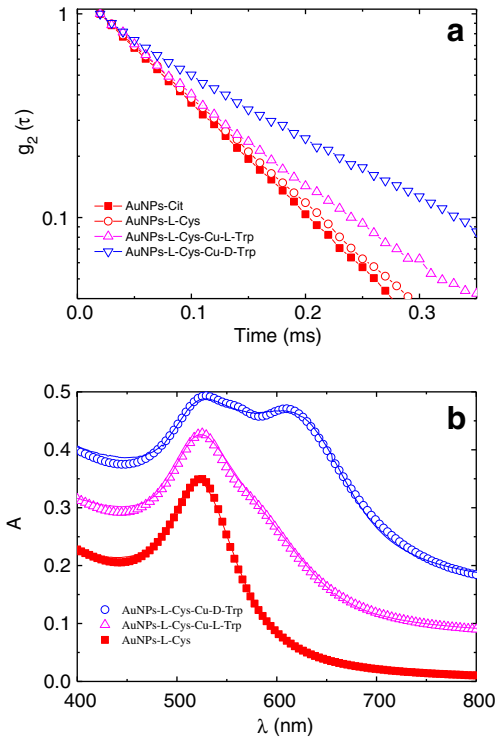

Fig. 7 **a** Correlation function $g2\ (\tau)$ for AuNPs citrate-capped, L-Cys-capped, AuNPs–L-Cys–Cu–L-Trp, AuNPs–L-Cys–Cu–D-Trp; **b** UV–Vis spectra of the systems AuNPs L-Cys-capped, AuNPs–L-Cys–Cu–L-Trp, AuNPs–L-Cys–Cu–D-Trp. The *solid lines* refer to fit obtained by Mie–Gans model

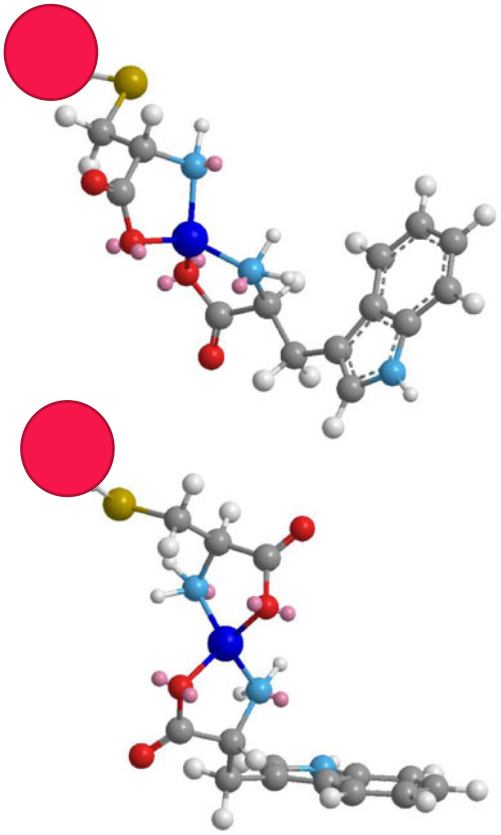

Fig. 8 Schematic descriptions of **a** L-Cys–Cu–L-Trp; **b** L-Cys–Cu–D-Trp

obtained for the systems AuNPs–L-Cys–Cu–L-Ala, AuNPs–L-Cys–Cu–D-Ala and AuNPs–L-Cys–Cu–D-Trp (Fig. 3a, b, d, respectively) evidence two SPR at 522 and 656 nm, respectively, indicating the formation of non spherical nanoparticles during the aggregation. Different authors [24, 64, 65] have shown that the Mie–Gans model is suitable for the evaluation of the size, shape, and fraction of nonspherical particles in a gold colloid by the simulation and fitting of the extinction spectra.

In our case, it is possible to consider the colloidal suspension as a mixture of spherical and ellipsoidal nanoparticles, and assuming that at low gold solution concentration, the aggregates are far from each other and therefore scatter light in an independent way; the total extinction cross section is given by:

$$\sigma = \mathrm{Ns}\cdot\sigma_{\mathrm{sph}}(\lambda, d) + \mathrm{Ne}\cdot\sum_{\rho}\sigma_{\mathrm{ellips}}(\lambda, a, \rho)\cdot G(\rho) \qquad (4)$$

where Ns and Ne are the concentration of spherical and ellipsoidal nanoparticles respectively, while σ_{sph} and σ_{ellips} are their cross sections (in quadrupole approximation) which depend on the size of the (spherical) particle (d), the wavelength of the incoming light (λ), the aspect ratio $\left(\rho = \frac{\text{major axis}}{\text{minor axis}}\right)$ and the minor axis (a) of the considered ellipsoid. In our model, we have also considered that the ellipsoids have, in the sol, a Gaussian distribution of aspect ratios $G(\rho)$, centered at ρ with a standard deviation s. Details

for the mathematical expressions of σ_{sph}, and σ_{ellips} can be found in Ref. [66]. Moreover, in our model, the minor ellipsoid axis was fixed to the diameter of the individual nanoparticle, which is 18 nm (as found with Haiss method).

The fitting procedure involves only a limited number of parameters (Ns, Ne, ρ, σ) and in Fig. 7b the experimental UV–Vis spectra and the calculated fits of the AuNPs–L-Cys–Cu–L-Trp, AuNPs–L-Cys–Cu–D-Trp and of AuNPs–L-Cys are shown. For the AuNPs–L-Cys system, the fit was obtained with a value of 18 nm for the nanoparticle diameter and an aspect ratio $\rho = 1.0$, because of the spherical nanoparticle shape. In the AuNPs–L-Cys–Cu–D-Trp system the UV–Vis spectrum was fitted with two distributions: a narrow distribution centered around $\rho = 1.0$, associated to the non aggregated nanoparticles and a broader distribution centered at $\rho = 0.45$ arising from aggregated nanoparticles. The major axis of ellipsoids results 40 nm, rather close the value obtained with DLS measurements. Also for the AuNPs–L-Cys–Cu–L-Trp, the spectrum fit was obtained with the same two distribution as in the case of AuNPs–L-Cys–Cu–D-Trp, however, in the last case the concentration of ellipsoids (Ne) was lower (about one order of magnitude).

The data obtained by the fitting of the extinction spectra and by the DLS measurements clearly show that whereas for L-Trp, where only a slight aggregation occurs, the major part of the nanoparticles remain spherical, for all the other investigated amino acids (L-Ala, D-Ala, and D-Trp) the aggregation processes mainly give rise to ellipsoidal nanoparticles, allowing us to shed some light on the enantiodiscrimination process. In fact, the different size of the alanine and tryptophan side chains is responsible for the different aggregation trends observed. Owing to its short side chain, the steric encumbrance of the ternary species of the alanine bound on the AuNPs surface is independent from the amino acid chirality. On the other hand, for the species formed by L- or D-Trp, the bulkier indolic residue plays a crucial role in the formation of the spheroidal nanoparticles. As shown in Fig. 8, in the homochiral species, the side chain of the amino acid points outwards the copper(II) coordination plane, disadvantaging the aggregation process; whereas in the heterochiral species, the indolic residue lies in the coordination plane, promoting the formation of non spherical aggregated particles. Moreover, in the AuNPs–L-Cys–Cu–D-Trp system the indolic group in the side chain is arranged in such a way (Fig. 8) that it could interact with other indolic groups present in the functionalized nanoparticles by multiple π–π interactions [67–70].

Conclusions

In this paper, we have shown that the unique properties of AuNPs can be smartly exploited to realize the enantiodiscrimination of D,L-Trp and of D,L-His. The knowledge of the solution equilibria allows us to settle a novel approach in this field. In fact, the calculation of the concentrations of the species present in solution enables a fine tuning of the experimental conditions and, as a consequence, the optimization of the discrimination process. Furthermore, the combination of different techniques (UV–Vis spectroscopy and DLS) allows us a deep understanding of the phenomena occurring in solution and to hypothesize different molecular pathways, as well as to shed light on the copper(II) ion pivotal role.

Acknowledgements We thank Valeria Zito (Istituto CNR di Biostrutture e Bioimmagini, Catania, Italy) for technical assistance and thank Università di Catania (Progetti di Ricerca di Ateneo) for financial support.

References

1. Blackmond DG (2011) The origin of biological homochirality. Phil Trans R Soc B 366:2878–2884
2. Kitagawa F, Otsuka K (2011) Recent progress in capillary electrophoretic analysis of amino acid enantiomers. J Chromatogr B 879: 3078–3095
3. Reischl RJ, Lindner W (2012) Methoxyquinoline labeling—a new strategy for the enantioseparation of all chiral proteinogenic amino acids in 1-dimensional liquid chromatography using fluorescence and tandem mass spectrometric detection. J Chromatogr A 1269: 262–269
4. Visser WF, Verhoeven-Duif NM, Ophoff R, Bakker S, Klomp LW, Berger R, de Koning TJ (2011) A sensitive and simple ultra-high-performance-liquid chromatography–tandem mass spectrometry based method for the quantification of D-amino acids in body fluids. J Chromatogr A 1218:7130–7136
5. Miyoshi Y, Koga R, Oyama T, Han H, Ueno K, Masuyama K, Itoh Y, Hamase K (2012) HPLC analysis of naturally occurring free d-amino acids in mammals. J Pharm Biomed Anal 69:42–49
6. Tojo Y, Hamase K, Nakata M, Morikawa A, Mita M, Ashida Y, Lindner W, Zaitsua K (2008) Automated and simultaneous two-dimensional micro-high-performance liquid chromatographic determination of proline and hydroxyproline enantiomers in mammals. J Chromatogr B 875:174–179
7. Blennow K, Hampel H, Weiner M, Zetterberg H (2010) Cerebrospinal fluid and plasma biomarkers in Alzheimer disease. Nat Rev Neurol 6:131–144
8. Cedazo-Minguez A, Winblad B (2010) Biomarkers for Alzheimer's disease and other forms of dementia: clinical needs, limitations and future aspects. Exp Gerontol 45:5–14
9. Samakashvili S, Ibáñez C, Sim C, Gil-Bea FJ, Winblad B, Cedazo-Mínguez A, Cifuentes A (2011) Analysis of chiral amino acids in cerebrospinal fluid samples linked to different stages of Alzheimer disease. Electrophoresis 32:2757–2764
10. Zhang Q, Guo L, Huang Y, Wang Y, Han Q, Fu Y (2013) A reagentless enantioselective sensor for tryptophan enantiomers via nanohybrid matrices. Anal Methods 5:4397–4401
11. Bai L, Romanova EV, Sweedler JV (2011) Distinguishing endogenous D-amino acid-containing neuropeptides in individual neurons using tandem mass spectrometry. Anal Chem 83:2794–2800
12. Iizuka H, Hirasa Y, Kubo K, Ishii K, Toyo'okab T, Fukushima T (2010) Enantiomeric separation of D, L-tryptophan and D, L-kynurenine by HPLC using pre-column fluorescence derivatization with *R*(−)-DBD-PyNCS. Biomed Chromatogr 25:743–747

13. Fleischer H, Thurow K (2013) Fast mass spectrometry-based enantiomeric excess determination of proteinogenic amino acids. Amino Acids 44:1039–1051
14. Glover CN, Hogstrand C (2002) Amino acid modulation of in vivo intestinal zinc absorption in freshwater rainbow trout. J Exp Biol 205: 151–158
15. Illangasekare M, Turk R, Peterson GC, Lladser M, Yarus M (2010) Chiral histidine selection by D-ribose RNA. RNA 16:2370–2383
16. Daniel MC, Astruc D (2004) Gold nanoparticles: assembly, supramolecular chemistry, quantum-size-related properties, and applications toward biology, catalysis, and nanotechnology. Chem Rev 104: 293–346
17. Mieszawska AJ, Mulder WJM, Fayad ZA, Cormode DP (2013) Multifunctional gold nanoparticles for diagnosis and therapy of disease. Mol Pharmaceutics 10:831–847
18. Mancin F, Prins LJ, Scrimin P (2013) Catalysis on gold-nanoparticle-passivating monolayers. Curr Opin Colloid Interface Sci 18:61–69
19. Wang C, Yu C (2013) Detection of chemical pollutants in water using gold nanoparticles as sensors: a review. Rev Anal Chem 32:1–14
20. Zhang M, Ye BC (2011) Colorimetric chiral recognition of enantiomers using the nucleotide-capped silver nanoparticles. Anal Chem 83:1504–1509
21. Sun Y, Zhang L, Li H (2012) Chiral colorimetric recognition of amino acids based on silver nanoparticle clusters. New J Chem 36: 1442–1444
22. Ghosh S, Hui Fang T, Uddin MS, Hidajata K (2013) Enantioselective separation of chiral aromatic amino acids with surface functionalized magnetic nanoparticles. Coll Surf B: Biointerfaces 105:267–277
23. Maoz BM, Chaikin Y, Tesler AB, Elli OB, Fan Z, Govorov AO, Markovich G (2013) Amplification of chiroptical activity of chiral biomolecules by surface plasmons. Nano Lett 13:1203–1209
24. Amendola V, Meneghetti M (2009) Size evaluation of gold nanoparticles by UV–vis spectroscopy. J Phys Chem C 113:4277–4285
25. Zimbone M, Calcagno L, Messina E, Baeri P, Compagnini G (2011) Dynamic light scattering and UV–vis spectroscopy of gold nanoparticles solution. Mater Lett 65:2906–2909
26. Maccarrone G, Contino A, Cucinotta V (2012) The study of solution equilibria in chiral capillary electrophoresis by the ligand-exchange mechanism. Trends Anal Chem 32:133–153, and references therein
27. Contino A, Cucinotta V, Giuffrida A, Maccarrone G, Messina M (2008) Synthesis and characterisation of the 3-amino-derivative of γ-cyclodextrin, showing receptor ability and metal ion coordination properties. Tetrahedron Lett 49:4765
28. Cucinotta V, Contino A, Giuffrida A, Maccarrone G, Messina M (2010) Application of charged single isomer derivatives of cyclodextrins in capillary electrophoresis for chiral analysis. J Chromatogr A 1217:953–967
29. Contino A, Maccarrone G, Remelli M (2013) Exploiting thermodynamic data to optimize the enantioseparation of underivatized amino acids in ligand exchange capillary electrophoresis. Anal Bioanal Chem 405:951–959
30. Giuffrida A, Caruso R, Messina M, Maccarrone G, Contino A, Cifuentes A, Cucinotta V (2012) Chiral separation of amino acids derivatised with fluorescein isothiocyanate by single isomer derivatives 3-monodeoxy-3-monoamino-β- and γ-cyclodextrins: the effect of the cavity size. J Chromatogr A 1269:360–365
31. Giuffrida A, Tabera L, Gonzàlez R, Cucinotta V, Cifuentes A (2008) Chiral analysis of amino acids from conventional and transgenic yeasts. J Chromatogr B 875:243–247
32. Giuffrida A, Contino A, Maccarrone G, Messina M, Cucinotta V (2011) Mass spectrometry detection as an innovative and advantageous tool in ligand exchange capillary electrophoresis. Electrophoresis 32: 1176–1181
33. Flaschka HA (1959) EDTA titrations. Pergamon, London, pp 78–79
34. Turkevich J, Stevenson PC, Hillier J (1951) A study of the nucleation and growth processes in the synthesis of colloidal gold. Discuss Faraday Soc 11:55–75
35. Frens G (1973) Controlled nucleation for the regulation of the particle size in monodisperse gold suspensions. Nature (London) Phys Sci 241:20–22
36. Hill HD, Mirkin CA (2006) The bio-barcode assay for the detection of protein and nucleic acid targets using DTT-induced ligand exchange. Nat Protoc 1:324–336
37. Wang S, Qian K, Bi XZ, Huang W (2009) Influence of speciation of aqueous $HAuCl_4$ on the synthesis, structure, and property of Au colloids. J Phys Chem C 113:6505–6510
38. Sethi M, Knecht MR (2009) Experimental studies on the interactions between Au nanoparticles and amino acids: bio-based formation of branched linear chains. Appl Mat Interfaces 1:1270–1278
39. Maye MM, Han L, Kariuki NN, Ly NK, Chan WB, Luo J, Zhong CJ (2003) Gold and alloy nanoparticles in solution and thin film assembly: spectrophotometric determination of molar absorptivity. Anal Chim Acta 496:17–27
40. Haiss W, Thanh NTK, Aveyard J, Fernig DG (2007) Determination of size and concentration of gold nanoparticles from UV–vis spectra. Anal Chem 79:4215–4221
41. Alderighi L, Gans P, Ienco A, Peters D, Sabatini A, Vacca A (1999) Hyperquad simulation and speciation (HySS): a utility program for the investigation of equilibria involving soluble and partially soluble species. Coord Chem Rev 184:311–318
42. Berne BJ, Pecora R (1976) Dynamic light scattering. Wiley, New York
43. Aryal S, Bahadur KCR, Bhattarai N, Kim CK, Kim HY (2006) Study of electrolyte induced aggregation of gold nanoparticles capped by amino acids. J Colloid Interface Sci 299:191–197
44. Ahrland S (1968) Thermodynamics of complex formation between hard and soft acceptors and donors. In Struc Bonding (Berlin, Germany) 5:118–149
45. Ghosh SK, Nath S, Kundu S, Esumi K, Pal T (2004) Solvent and ligand effects on the localized surface plasmon resonance (LSPR) of gold colloids. J Phys Chem B 108:13963–13971
46. Zhang FX, Han L, Israel LB, Daras JG, Maye MM, Ly NK, Zhong CJ (2002) Colorimetric detection of thiol-containing amino acids using gold nanoparticles. Analyst 127:462–465
47. Ping Li Z, Rui Duan X, Hui Liu C, Du An B (2006) Selective determination of cysteine by resonance light scattering technique based on self-assembly of gold nanoparticles. Anal Biochem 351: 18–25
48. Hormozi-Nezhada MR, Seyedhosseini E, Robatjazi H (2012) Spectrophotometric determination of glutathione and cysteine based on aggregation of colloidal gold nanoparticles. Scientia Iranica F 19: 958–963
49. Csapó E, Patakfalvi R, Hornok V, Tamás Tóth L, Sipos Á, Szalai A, Csete M, Dékány I (2012) Effect of pH on stability and plasmonic properties of cysteine-functionalized silver nanoparticle dispersion. Colloids Surface B 98:43–49
50. Nam J, Won N, Jin H, Chung H, Kim S (2009) pH-induced aggregation of gold nanoparticles for photothermal cancer therapy. J Am Chem Soc 131:13639–13645
51. Deng J, Yu P, Yang L, Mao L (2013) Competitive coordination of Cu^{2+} between cysteine and pyrophosphate ion: toward sensitive and selective sensing of pyrophosphate ion in synovial fluid of arthritis patients. Anal Chem 85:2516–2522
52. Jiang L, Guan J, Zhao L, Li J, Yang W (2009) pH-dependent aggregation of citrate-capped Au nanoparticles induced by Cu^{2+} ions: The competition effect of hydroxyl groups with the carboxyl groups. Colloid Surface A 346:216–220
53. Arena G, Bonomo RP, Casella L, Gullotti M, Impellizzeri G, Maccarrone G, Rizzarelli E (1991) Thermodynamic stereoselectivity assisted by weak interactions in metal complexes. Copper(II) ternary

complexes of cyclo-L-histidyl-L-histidine and L- or D-amino acids in aqueous solution. J Chem Soc Dalton Trans 3203–3209
54. Bonomo RP, Cucinotta V, D'Alessandro F, Impellizzeri G, Maccarrone G, Rizzarelli E (1993) Coordination properties of 6-deoxy-6-[1-(2-amino)ethylamino]-β-cyclodextrin and the ability of its copper(II) complex to recognize and separate amino acid enantiomeric pairs. J Inclus Phenomen 15:167–180
55. Corradini R, Dossena A, Impellizzeri G, Maccarrone G, Marchelli R, Rizzarelli E, Sartor G, Vecchio G (1994) Chiral recognition and separation of amino acids by means of a copper(II) complex of histamine monofunctionalized β-cyclodextrin. J Am Chem Soc 116:10267–10274
56. Bonomo RP, Cucinotta V, Maccarrone G, Rizzarelli E, Vecchio G (2001) Thermodynamic stereoselectivity assisted by weak interactions in metal complexes. Chiral recognition of L/D-amino acids by the copper(II) complex of 6-deoxy-6-[4-(2-aminoethyl)imidazolyl]-cyclomaltoheptaose. J Chem Soc Dalton Trans 1366–1373
57. Dallavalle F, Folesani G, Sabatini A, Tegoni M, Vacca A (2001) Formation equilibria of ternary complexes of copper(II) with (*S*)-tryptophanhydroxamic acid and both D- and L-amino acids in aqueous solution. Polyhedron 20:103–109
58. Cucinotta V, Giuffrida A, Maccarrone G, Messina M, Puglisi A, Rizzarelli E, Vecchio G (2005) Coordination properties of 3-functionalized β-cyclodextrins. Thermodynamic stereoselectivity of copper(II) complexes of the A,B-diamino derivative and its exploitation in LECE. Dalton Trans 2731–2736
59. Wagener P, Schwenke A, Barcikowski S (2012) How citrate ligands affect nanoparticle adsorption to microparticle supports. Langmuir 28:6132–6140
60. Daniele PG, Ostacoli G (1976) Ternary complexes formation between Cu^{2+} ion, citric acid and L-histidine, or histamine in aqueous solution. Ann Chim 387:387–399
61. Arena G, Calì R, Cucinotta V, Musumeci S, Rizzarelli E, Sammartano S (1983) Thermodynamics of metal complexes with ligand–ligand interaction, simple and mixed complexes of copper(II) and zinc(II) with adenosine 5'-triphosphate and L-tryptophan or L-alanine. J Chem Soc Dalton Trans 1271–1278
62. Zimbone M, Musumeci P, Baeri P, Messina E, Boninelli S, Compagnini G, Calcagno L (2012) Rotational dynamics of gold nanoparticle chains in water solution. J Nanopart Res 14:1308–1318
63. Zimbone M, Calcagno L, Baeri P, Messina GC, Compagnini G (2012) Dynamic light scattering in gold colloids prepared by laser ablation in water. Appl Surf Sci 258:9246–9249
64. Galletto P, Brevet PF, Girault HH, Antoine R, Girault HG (1999) Enhancement of the second harmonic response by adsorbates on gold colloids: the effect of aggregation. J Phys Chem 103:8706–8710
65. Rouillat MH, Antoine R, Benichou E, Brevet P (2001) Resonant hyper Rayleigh scattering of single and aggregated gold nanoparticle. Anal Sci 17:i235–i238
66. Bohren CF, Huffman DR (2004) Absorption and scattering of light by small particles. Wiley, Chichester, UK
67. Yajima T, Maccarrone G, Takani M, Contino A, Arena G, Takamido R, Hanaki M, Funahashi Y, Odani A, Yamauchi O (2003) Combined effects of electrostatic and π–π stacking interactions: selective binding of nucleotides and aromatic carboxylates by platinum(II)—aromatic ligand complexes. Chem Eur J 9:3341–3352
68. Yajima T, Takamido R, Shimazaki Y, Odani A, Nakabayashi Y, Yamauchi O (2007) π–π Stacking assisted binding of aromatic amino acids by copper(II)–aromatic diimine complexes. Effects of ring substituents on ternary complex stability. Dalton Trans 299–307
69. Shimazaki Y, Yajima T, Takani M, Yamauchi O (2009) Metal complexes involving indole rings: structures and effects of metal–indole interactions. Coord Chem Rev 253:479–492
70. Teklebrhan RB, Ge L, Bhattacharjee S, Xu Z, Sjoblom J (2012) Probing structure-nanoaggregation relations of polyaromatic surfactants: a molecular dynamics simulation and dynamic light scattering study. J Phys Chem B 116:5907–5918